J. Fluid Mech. (1983), *vol.* 132, *pp.* 319–336
Printed in Great Britain

A spanwise structure in the plane shear layer

By JAVIER JIMENEZ

IBM Scientific Center, P. Castellana 4, Madrid, Spain and School of Aeronautics, Universidad Politecnica, Madrid

(Received 1 September 1981 and in revised form 10 March 1983)

We study experimentally the spanwise structure of the mean flow field of a plane shear layer. The field is dominated by a lateral undulation that persists downstream to form long longitudinal structures. Both the amplitude and spacing of these structures vary in such a way as to suggest that they are due to a secondary instability of the flow field. Some models for this instability are discussed and compared with the experimental results.

1. Introduction

An important question in the development of the plane mixing layer is the mechanism of appearance of three-dimensionality in the flow. This has usually been taken to mean the generation of a Kolmogorov-type small-scale cascade, but lately there has been some evidence of a large-scale spanwise instability of the layer as a whole. Konrad (1976) and Breidenthal (1981) observed longitudinal streaks in pictures of the concentration field of mixing layers, which can be interpreted as corrugations of the vortex cores (Bernal *et al.* 1979). Browand & Troutt (1980) found three-dimensional effects in the vortex amalgamation process, and Roshko (1980) has reported evidence of the presence of longitudinal vortices in the flow. Recently, Bernal (1981) has published pictures showing longitudinal concentration structures that strongly support this last interpretation. Our measurements refer to the spanwise (z) structure of the mean-flow properties.

We study a rectangular half-jet in air and use a hot-wire anemometer to measure the mean longitudinal velocity and turbulence level fields. By exploring the flow along the three coordinate axes, we are able to detect spanwise variations that can be interpreted as showing that the shear layer as a whole suffers a transversal spanwise undulation, both in the average velocity field and in the turbulent intensity. The wavelength and magnitude of this undulation evolves downstream in a way that is suggestive of the development of an instability.

Most of the development happens in what could be called the transition region of the shear layer, corresponding to the first few pairing events of the large structure. Since it might be expected that events in this region are governed by scales related to the thickness of the initial boundary layer, we have studied two cases with rather different free-stream velocities (16–51 m/s), and with correspondingly different boundary-layer thicknesses. The effect of scaling both on the transition and on the spanwise structure is examined in some detail. Finally, we discuss the results in the light of some of the different models that have been offered to account for the three-dimensional instability of the shear layer.

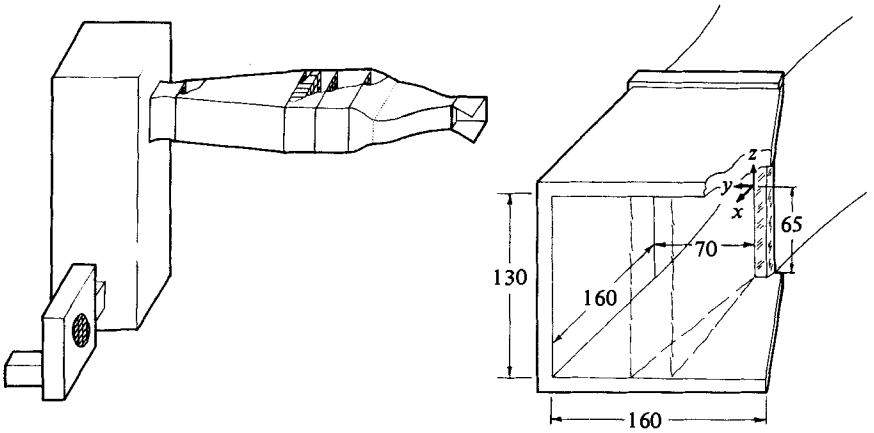

FIGURE 1. Sketch of the experimental apparatus and test section, showing the distribution of screens and flow straighteners. Dimensions are in mm.

2. Experimental arrangement and flow description

A sketch of the experimental apparatus is given in figure 1. The output from a centrifugal blower goes through a large (0.35 m^3) settling chamber, an 8° diffuser and a series of screens and flow straighteners into a 10:1 contraction, discharging into a large room through a rectangular nozzle. The diffuser is separated from the settling chamber by a flexible cloth section which effectively isolates the mechanical vibration of the blower from the test section. The centrifugal blower is powered by a constant speed AC motor, and the flow rate can only be controlled by changing the amount of dissipation in the tunnel; the two different speeds used in this experiment were achieved by introducing a perforated plate in front of the blower intake.

Since it was realized that the spanwise variation of the flow could be due to defects in the tunnel construction, the whole apparatus was taken apart and rebuilt several times in the course of the experiment. This redesign involved quite extensive rearrangements of the size and number of screens and flow straighteners and a substantial increase in the volume of the settling chamber. The description given here relates to the final series of measurements, but the qualitative nature of the results, including the basic scales of the flow, did not seem to be very much affected by the changes.

The configuration of the nozzle is shown in the right-hand side of figure 1, which also defines the coordinate system used throughout the paper. The active lip of the nozzle is a milled plastic rectangular block. The block was mounted on the wooden nozzle, and both parts were carefully sanded together to a smooth finish all the way up to the first tunnel screen; then they were lacquered and polished several times until the surface was optically shiny and the step between the nozzle and the block could not be felt by touch. Once during the experiment the whole nozzle was reworked, sanded and lacquered; while this avoided a particular strong local undulation of the flow field, the basic wavelength and amplitude of the deformation were not affected by the change. The arrangement of all the physical pieces of apparatus in the proximity of the jet, including the observer, was changed repeatedly until it was clear that no outside interference was the cause of the spanwise nonuniformity.

Instantaneous measurements of the longitudinal velocity were taken using com-

U_1 (m/s)	u'/U_1 stream	u'/U_1 boundary layer	λ_{z0} (mm)	θ (mm)	$\frac{U_1\theta}{\nu}$	$\frac{d\delta_\omega}{dx}$	$\frac{x_0}{\theta}$	Symbol
16	0.006	0.035	6.22	0.204	220	0.22	−60	○
51	0.003	0.014	4.80	0.127	430	0.14	−240	×

TABLE 1

mercial hot-wire equipment (DISA), holding the probe support at 45° from the stream to minimize interference effects. The probe was traversed using a triaxial movement which was operated manually. The positional precision of the movement was 0.05 mm, and its repeatability and linearity were checked to be better than 0.1 mm. The hot-wire output was digitized to an accuracy of ten bits every 5 ms and reduced digitally to velocity; each average and standard deviation was computed from 1000 samples. Each of the maps given below is the result of between 200 and 400 such average values distributed more or less uniformly across the plane; the computation of the isolines was done using cubic-splines interpolation.

Some power spectra of the velocity fluctuations were also obtained, both to track the evolution of the small-scale transition and to obtain the basic period of the large-scale eddies. For this purpose the output of the anemometer was sampled at 100 KHz during 5 s, each sample reduced individually to velocity, and the spectra computed digitally using an averaged windowed FFT method (Welch 1967).

The free-stream turbulence level in the jet changed somewhat with the different configurations of the tunnel. At its worst, in the early experiments at 16 m/s, it was slightly below 0.6 %, with much of the power concentrated at the blower rotation frequency (48 Hz), while in the final configuration it was about 0.3 %, with most of the power in the form of broadband noise. The low-speed stream was entrained directly from the room, and, even if a point was made of working only on days in which nobody but the observer was in the laboratory, it probably contributed most of the input turbulence. The boundary layer at the nozzle lip was laminar in all cases, although with a Reynolds number close to the transition region; its measured momentum thickness θ agreed quite closely with the one computed from the shape of the contraction. The top turbulence level u'/U_1 within the boundary layer was 3.5 % in the low-speed experiments, and 1.4 % in the high-speed ones (which used also the cleaner configuration). Presumably as a result (Hussain & Zedan 1978) the spreading rate of the shear layer was quite different in both cases; thus while the growth rate of the vorticity thickness

$$\delta_\omega = \frac{U_1}{\partial U/\partial y_{\max}}$$

was about 0.22 in the first case, it was only 0.14 in the second. A summary of the parameters of the two layers is given in table 1.

Although results from both layers are used in this paper, all of the detailed maps presented refer to the fast one. The qualitative behaviour is the same in both cases, and maps of the low-speed layer can be found in (Jimenez, Martinez-Val & Rebollo 1979*b*), which constitutes an early report on this work.

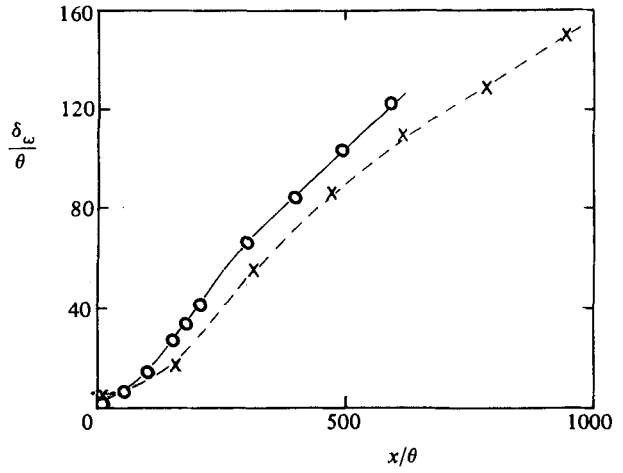

FIGURE 2. Evolution of the vorticity thickness. For symbols see table 1.

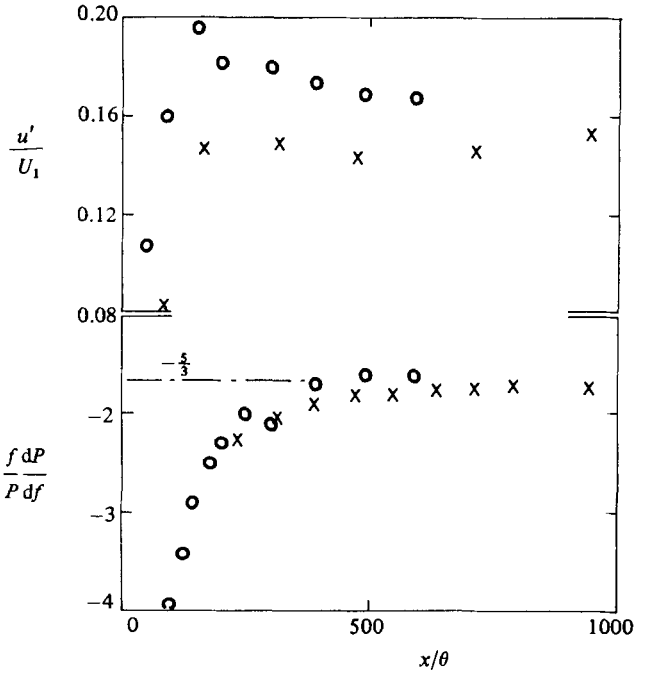

FIGURE 3. Evolution of maximum turbulence level (top) and log slope of spectrum in inertial subrange (bottom). For symbols see table 1.

3. The two-dimensional evolution

The main purpose of this section is to characterize the basic two-dimensional behaviour of the shear layers used in this experiment so as to give a frame of reference for the development of the spanwise variations discussed below. Average velocity and longitudinal fluctuation-level profiles were obtained by scanning with the hot wire the midspan (x, y)-plane. Since the region of interest is the transition from the linear-instability stage to the fully developed turbulent one, all the data are presented

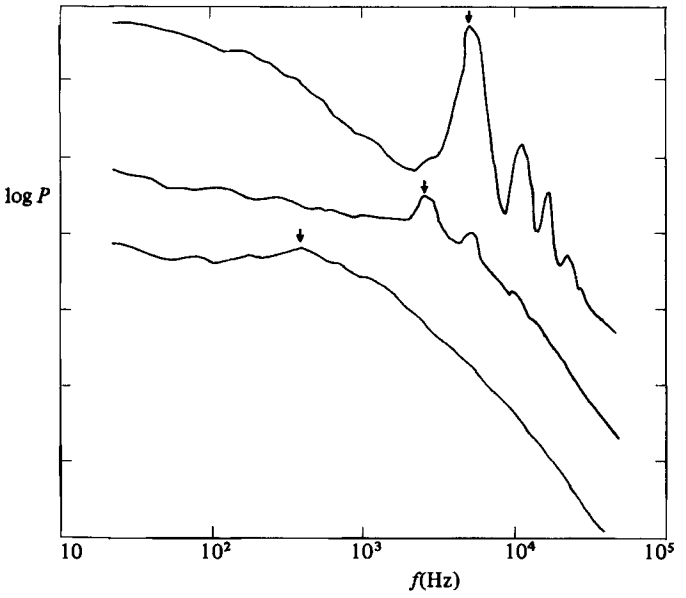

FIGURE 4. Examples of power spectra. The top two spectra are near the nozzle ($x = 10$, 20 mm), bottom one is at $x = 60$ mm. Note the pairing between first two spectra and differences in slope of the inertial subrange. $U_1 = 51$ m/s; $U/U_1 = 0.5$.

normalized with the momentum thickness of the nozzle boundary layer. This length should fix the scale of the initial instability and of the transition region. In fact, the correspondence between the two experiments can be made somewhat closer by using as normalizing length the actual initial wavelength λ_{20} of the primary two-dimensional instability, but we have kept the more classical normalization to facilitate comparison with previous investigations.

The downstream growth of the vorticity thickness is given in figure 2. As noted above the two different growth rates (computed for x above 400 θ) are probably due to the different levels of disturbance in the nozzle boundary layer, and they correspond quite well to the ones given by Hussain & Zedan (1978) for unperturbed and tripped laminar layers; these measurements may not be too significant, in any case, since none of the layers has a very long self-preserving region. The shape of the growth curve is typical of the ones given in that reference for laminar layers and the length of the transition region (300–400 θ) also agrees well with their results.

The top part of figure 3 gives the evolution of the maximum longitudinal turbulence level. The transition region in this case is also about 300 θ. The bottom part of the same figure gives some insight into the behaviour of the small scale during transition. As the layer approaches a fully turbulent state, the power spectrum of the longitudinal velocity fluctuation develops an inertial subrange whose slope, when plotted in logarithmic scale, should approach the Kolmogorov value of $-\frac{5}{3}$. During the initial part of the development the inertial subrange is also present but its slope is steeper (Jimenez, Martinez-Val & Rebollo 1979*a*), reflecting the decreased efficiency of the dissipation cascade in that region. The slopes given in figure 3 were obtained from spectra taken in the midspan plane and deep inside the layer ($U/U_1 = 0.5$); the rise to the equilibrium value is quite clear and scales well with the momentum thickness, although the transition length is somewhat longer than in the previous cases (500 θ).

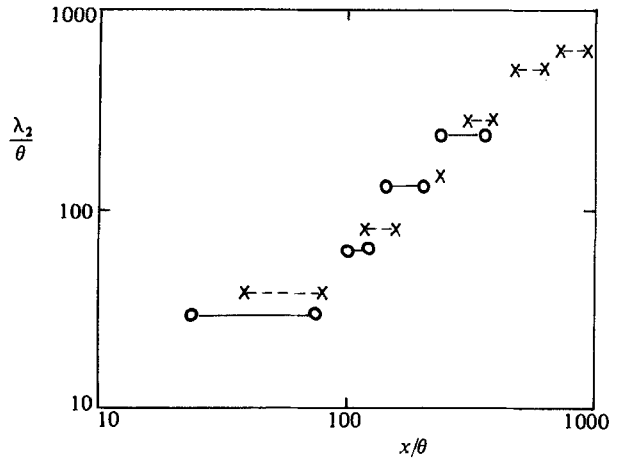

FIGURE 5. Evolution of dominant two-dimensional large-structure wavelength. For symbols see table 1.

The periodicity of the large eddies can also be studied using the fluctuation spectra. In the region near the nozzle exit the spectra contain strong peaks that permit the easy identification of the important frequencies which can usually be checked by direct inspection of the anemometer output; further downstream these peaks disappear and the only remaining clue is a 'knee' in the slope of the power spectrum (see figure 4). While it is not absolutely clear that this 'knee' represents the same quantity as the peaks in the spectra of the initial region, we have used it in that way. The results are given in figure 5, where the passing frequencies have been reduced to eddy wavelengths using the theoretical convection velocity $\frac{1}{2}U_1$. Not only the wavelength of the initial instability, but also the position of the first pairing (90 θ), and less accurately the second one (150 θ), are seen to scale with the momentum thickness. The initial wavelength agrees roughly with the theoretical value (29 θ) given by Michalke (1965), and, using only those points beyond 300 θ, a least-square fit gives

$$\frac{\lambda_2}{x} = 0.561\,\alpha, \quad \alpha = \frac{U_1 - U_2}{U_1 + U_2},$$

which agrees very well with the values (averaging to 0.563 ± 0.02) found for this quantity by direct eddy counting in Winant & Browand (1974), Koochesfahani *et al.* (1979), Bernal (1981) and Hernan & Jimenez (1982).

4. The spanwise structure

When the anemometer probe is traversed parallel to the span of the layer (z) it is evident that there are large non-uniformities in the flow. Three such traverses, each one of them at constant x and y, are shown in figure 6, and the non-uniformities are apparent both in the mean velocity and the turbulence level, taking the form of a roughly sinusoidal variation. By sampling the flow in planes perpendicular to the flow velocity, it is possible to gain a better idea of the structure of this variation; in fact it is possible to construct isolines giving the shape of the mean-velocity field. Three such maps, corresponding to different constant values of x, are shown in figure 7; the first one is taken just downstream of the nozzle lip, and gives an idea of the flow conditions in the initial boundary layer. In this map, and in those taken in the region

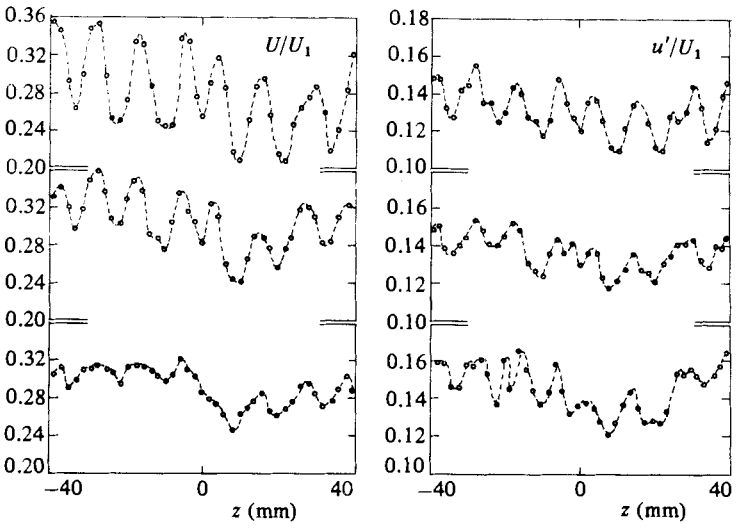

FIGURE 6. Spanwise distribution of mean velocity (left) and turbulence levels at three different positions in the shear layer. $x = 40$ (top), 60, 80 mm; $U_1 = 51$ m/s; $U/U_1 = 0.3$.

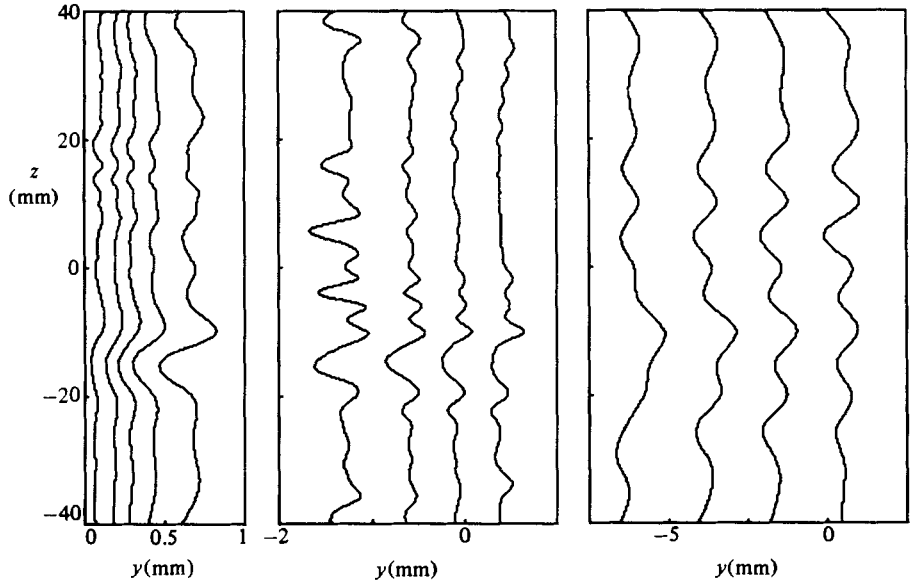

FIGURE 7. Mean velocity isolines in three transversal sections of the layer. $U_1 = 51$ m/s; $x = 1$ (left), 20, 60 mm. Isolines are $U/U_1 = 0.1$, 0.3, 0.5, 0.7, 0.9 for $x = 1$ and $U/U_1 = 0.2$, 0.4, 0.6, 0.8 for the other two maps. High-velocity stream is always on the right.

in which the layer is very thin, the actual shape of the nozzle edge is important; it is difficult to machine and maintain an edge that is completely straight over a length of 100 mm, and small deviations of tenths of a millimetre are substantial when compared with the momentum thickness of the initial boundary layer. The physical shape of the edge is, however, easily measured and taken into account, and the coordinate system used in all the maps in this paper is taken parallel to the nozzle edge, instead of strictly straight. The curvature of the edge varied throughout the

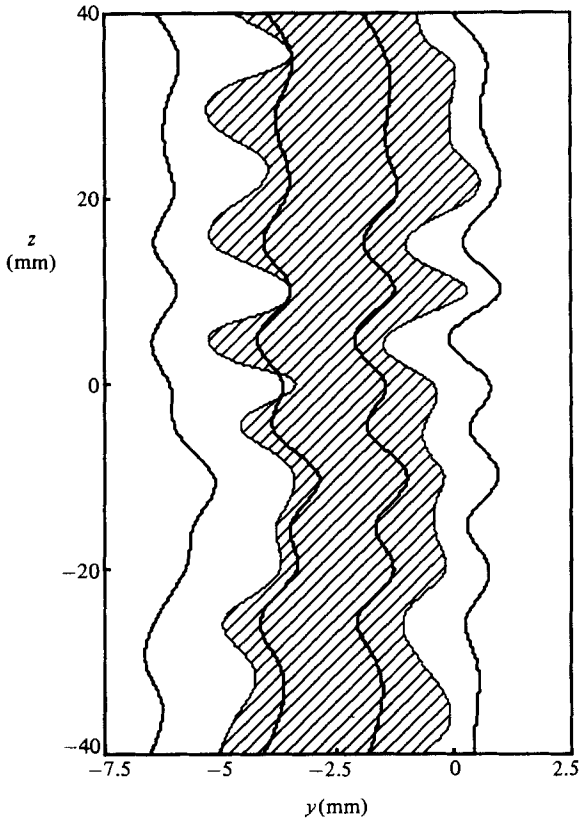

FIGURE 8. Comparison of transversal mean-velocity and turbulence-level maps. Mean-velocity map is the same as rightmost case in figure 7. Shaded region is $u'/U > 0.14$.

experiment, since the nozzle lip was reworked twice. The r.m.s. deviation from straightness was between 0.05 and 0.08 mm, distributed with a wavelength of the order of 40 mm in such a way that the maximum slope was never bigger than 1 %. Even so, the strong feature that can be seen in the lower half of the left-hand side map of figure 7 was associated to a particularly sharp corner in the edge.

The nature of the spanwise variation is seen to be a lateral deformation of the layer as a whole, such that its amplitude and shape are comparatively constant across a transversal section of the layer although they change from one section to another. The information contained in the turbulent intensity field confirms this interpretation, as can be seen in figure 8, which shows one intensity isoline superimposed to the average velocity field. The two fields have the same general shape, but the fact that the amplitude of the deformation is not the same in both cases proves that the layer is not only bent but internally deformed as well. The transversal (y) coordinate of all these maps is stretched, but the isolines span much of the thickness of the layer and they should give an idea of the magnitude of the deformation with respect to that thickness.

The downstream evolution of the deformation can also be studied by appropriate sampling. A good representative magnitude is the shape of a constant mean-velocity isosurface; if there were no spanwise variation this surface would be a cylinder whose generator would be everywhere parallel to the nozzle edge, and any deviation from

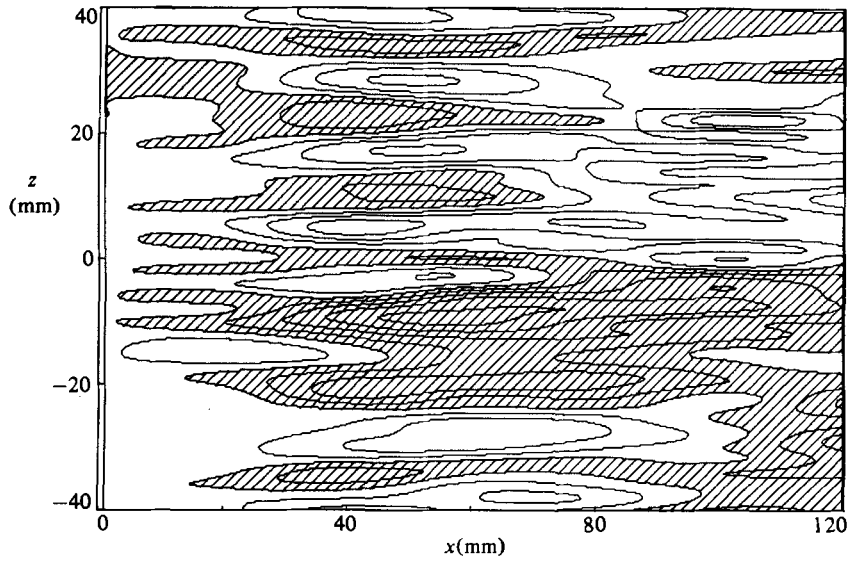

FIGURE 9. Topography of equal-mean-velocity surface $U/U_1 = 0.3$. Shaded regions are deformed towards high-speed side. Distance between contour lines is 0.2 mm.

the parallelism represents an undulation. A map of the isosurface $U/U_1 = 0.3$ is given in figure 9. The shaded regions are deformed towards the high-speed side of the layer, while the clear ones are deformed towards the low-speed one. The results are strikingly reminiscent of the longitudinal streamers observed in time-averaged concentration pictures by Konrad (1976) and Breidenthal (1981), and they show that the deformation has a fairly long spatial coherence as well as an amazing constancy in time.

It seems clear that some kind of locking to upstream disturbances is needed to explain this constancy, and a vigorous search was done to identify them; in some cases, all of them corresponding to especially strong features, this could be achieved. In one case a streamer originated in a small non-uniformity of the most downstream screen in the tunnel while in others, like the one in figure 7, they were associated with nicks in the nozzle lip. In fact it was easy to produce artificial streamers by introducing small obstacles just downstream of the lip, and these streamers looked very similar to the natural ones, although typically much stronger.

Most streamers, however, could not be ascribed to a definite cause, and the fact that their spacing changes as they move downstream suggests that they are not just remainders of upstream influences. For example, the series of closely spaced streamers that can be seen in the left (upstream) part of figure 9 coalesce later into bigger ones in what appear in some cases to be amalgamations and, still later, disappear or amalgamate again to form still wider undulations.

The evolution of the average spanwise wavelength of the corrugation is shown in figure 10; as far as possible the wavelength has been measured using complete (y, z)-maps like the ones shown in figure 7, but, in some cases, they have been deduced from single z-scans, usually near $U/U_1 = 0.3$. The wavelengths were computed by averaging the distances between a few pairs of clearly visible maxima and minima, and the scatter among pairs was usually not too large. The results follow the same pattern in both experiments; after beginning at a relatively large value, the

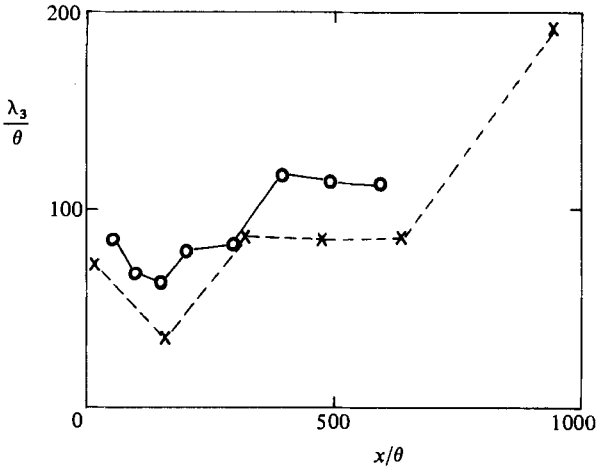

FIGURE 10. Evolution of spanwise wavelength. For symbols see table 1.

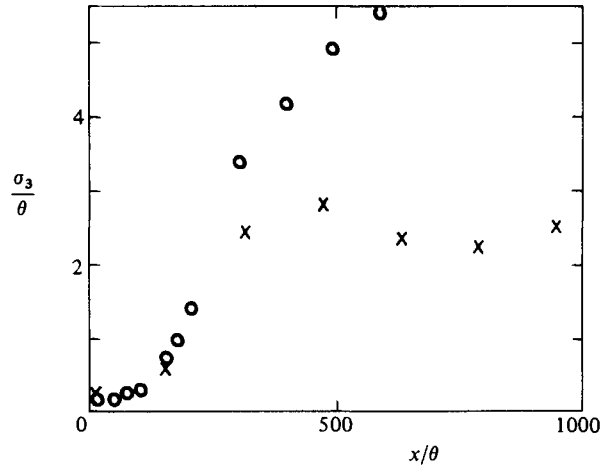

FIGURE 11. Evolution of spanwise amplitude. For symbols see table 1. $U/U_1 = 0.3$.

wavelength decreases, and, after 100 momentum thickness, begins to grow again, with the growth occurring in a series of discontinuous jumps which correspond to the disappearance of one or several streamers. It will be seen below that, upstream of the minimum, the amplitude of the undulation is too small for it to be significant. When only points downstream of 100 θ are considered, a least-square linear fit gives a growth rate of the spanwise wavelength,

$$\lambda_3/x = 0.26 \pm 0.09,$$

which is between 1 and 1.5 times faster than the growth of the vorticity thickness.

The amplitude of the undulation is also of interest. One way to characterize it is to give the r.m.s. value of the deviation of an equal-velocity isosurface from local parallelism to the nozzle lip. This downstream evolution of this magnitude is plotted in figure 11, which uses the 0.3 isosurface. Its variation across the layer is given in figure 12, which shows again that the deviation is fairly independent of y, and that the undulation is a deformation of the layer as a whole, at least in the downstream

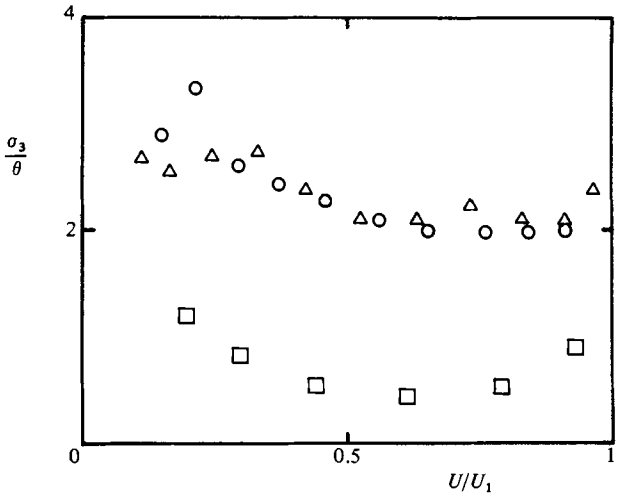

FIGURE 12. Spanwise amplitude variation across the layer. □, $x = 20$ mm; ○, 60; △, 120.

stations in which the undulation is well developed. Also in this case the length of 100 momentum thickness seems important; it is only downstream of that point that the undulation grows. The subsequent behaviour is different for both layers; even if in both cases the growth rate decreases after the initial development, the decrease is much more marked in the fast layer, in which the amplitude actually becomes almost constant. It is not clear what is the reason for this discrepancy, but, since the measured values are averages over a long time (a complete map takes a whole evening of observations), their amplitude must depend a lot on the locking of the features to the upstream disturbances, and this lock is presumably lost as we move downstream. It may be that the 'dirtier' boundary layer of the 16 m/s experiment provides a stronger lock than the cleaner one of the other case, and thus permits the observations of strong streamers at longer distances from the lip. Other interpretations are discussed below.

These observations can be compared with those of other investigators. Both Konrad (1976) and Bernal (1981) quote an average value for the spanwise wavelength equal to the local vorticity thickness, in good agreement with the one found in our case. Wygnasky *et al.* (1979) present measurements of spanwise correlation R_{vv} of the transversal velocity component, which can be used to infer a spanwise scale. Most of the correlation is lost in about 0.6 δ_ω, which, if interpreted as half a wavelength, will give a value consistent with the one above. In that same paper, spanwise correlations of temperature in a heated layer are presented which suggest a similar scale. Browand & Troutt (1980), on the other hand, present spanwise correlations of the longitudinal velocity component and flow visualizations which can be interpreted as giving a much longer coherence scale (6–9 δ_ω). This difference is important. What they observe is a branching structure in the amalgamation of the large eddies, which could be a different effect from the corrugation observed here. In fact the separation between probes in the rake they use for visualization is never smaller than $0.7\delta_\omega$, and usually quite a bit larger, and the scale of the phenomenon discussed here would be very difficult for them to observe. On the other hand, the downstream position they give for the growth of three dimensionality (300 θ) agrees well with the one found here.

Bernal finds that, for a wide range of velocity ratios in a He–N mixing layer, the

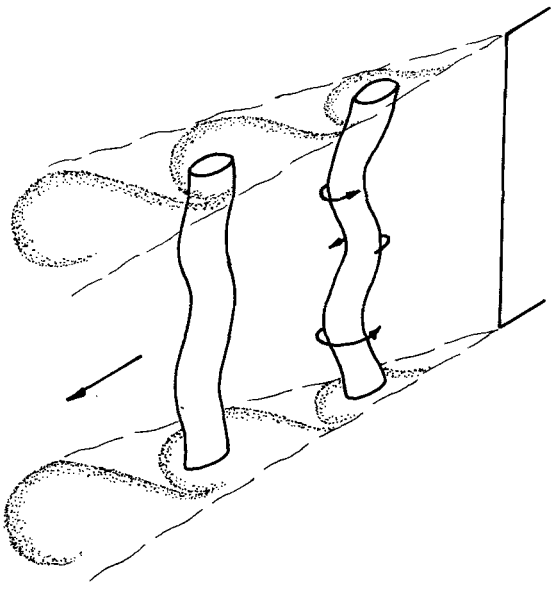

FIGURE 13. Sketch of proposed core deformation. Plane of deformation is inclined to free stream, and amplitude is arbitrary.

longitudinal structures become visible in his shadowgraphs at a point in which $\lambda_2 = 2\lambda_{20}$; this would correspond to about 150 θ in our experiment and is near the point where the spanwise amplitude begins to grow in figure 11. Breidenthal does not give any data for the point of inception of the corrugation in his pictures, but associates the appearance of three-dimensionality with a transition on the amount of mixing in his layer. He gives evidence that the point at which this transition is completed depends not only on the momentum thickness of the boundary layer but on the Reynolds number based on that thickness on the high-speed side of the splitter plate. He observes, however, that, for large Reynolds numbers comparable to the ones in our experiment, this point is close to 500 momentum thickness. This is consistent with the end of the small-scale transition in figure 3.

If we tentatively identify this point with the end of the transition regime, as suggested by the figure, we can compare it with measurements by Hussain & Zedan (1978); they also find that the transition length depends on the initial Reynolds number, following a pattern similar to that in Breidenthal, but settles to about 300 θ at large Reynolds. All these numbers are different and relate to different properties in the flow, but, taken together, they seem to imply that the end of transition in mixing layers with laminar initial boundary layers at high enough Reynolds numbers (> 200) occurs in the range of 300–500 θ, with different properties reaching equilibrium at slightly different points. This is consistent with our measurement on the growth of the corrugation.

5. Discussion

The observed deformation of the shear layer implies the presence of vorticity aligned in the transversal (y) direction, which, when added to the classical (z) component of vorticity in the two-dimensional cores, suggests a picture in which the cores themselves are deformed, or corrugated (see figure 13). This is precisely what

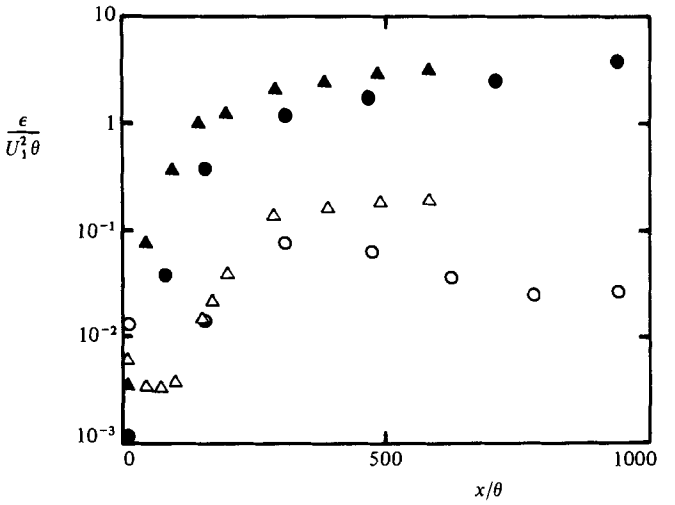

FIGURE 14. Evolution of the total energy associated to the two-dimensional flow (solid symbols) and the corrugation (open symbols). ○, $U_1 = 16$ m/s; △, 51 m/s.

Breidenthal observed in his concentration pictures, although he interpreted them as indications of longitudinal (x) vorticity. Actually, both interpretations are different but not incompatible; there is no reason to assume that the deformation of the vortex cores will happen precisely across or along the layer, and, in fact, it will be seen below that linear stability theory predicts a most unstable direction close to the axis of maximum strain, at 45° from the free stream. The recent laser fluorescence pictures obtained by Bernal (1981) (see also Roshko 1980) show longitudinal concentration structures which are aligned not only along but *across* the layer and may correspond to a later stage of the deformed cores postulated here.

We have stated above that the onset of this undulation has the characteristics of an instability. It is possible, from the experiments, to compute the total kinetic energy contained in the undulation and to compare its growth or decay with the energy in the fundamental two-dimensional mode. The latter, when integrated across the layer, is proportional to

$$\frac{\epsilon_x}{U_1^2\theta} = \frac{u'^2\delta_\omega}{U_1^2\theta},$$

while that in the three-dimensional mode is

$$\frac{\epsilon_z}{U_1^2\theta} = \left(\frac{\sigma_3 U_1}{\delta_\omega}\right)^2 \frac{\delta_\omega}{U_1^2\theta} = \frac{\sigma_3^2\delta_\omega}{\theta}.$$

Both quantities are plotted in figure 14. Especially in the 16 m/s layer, whose initial region is better documented, ϵ_z is seen actually to decrease from its initial value to increase later at a rate which is not too far below that of ϵ_x. Further downstream, both energies saturate. This behaviour supports the view that the undulation, though perhaps triggered by upstream influences, is a real instability with a growth rate comparable to the primary one. Moreover, this instability does not develop until the primary wave is well organized (100 θ).

Several mechanisms have been proposed for the origin of three-dimensional instabilities in parallel shear flows. Benney (1961), while trying to understand transition in the laminar boundary layer, studied the nonlinear interaction between

two- and three-dimensional waves in the inviscid free laminar shear layer. His mechanism implies the presence of pairs of counterrotating longitudinal vortices located symmetrically on both sides of the dividing streamline, and whose net effect is to produce a 'varicose' deformation in which the profile is alternatively thinner and thicker along the span. This is not observed in our experiments.

Saffman & Baker (1979), referring to the observations by the Caltech group, and elaborating on older ideas on the deformation of vortex rings (Widnall, Bliss & Tsai 1974), suggested that the phenomenon might depend on the presence of discrete cores. Although they do not develop a complete model, their proposed mechanism is the short-wave instability of a vortex filament on an external strain (Moore & Saffman 1975). As applied to a shear layer, each core sits in a straining field produced by all the other cores in the layer, and is deformed by it. The criterion for instability is that the self-induced rotation of the bent core be zero, in which case the effect of the imposed strain is cumulative and the deformation grows. For vortex cores with uniform vorticity distributions, the most-unstable wave has a wavelength 2.5 times greater than the core radius (Tsai & Widnall 1976), and, if we take the diameter of the cores in the shear layer to be the vorticity thickness, we get a wavelength of $1.25\,\delta_\omega$, which is in good agreement with the downstream behaviour of the data presented above. The predicted deformation is a plane sinusoidal undulation of the cores at 45° from the stream velocity, but its internal structure is more complicated than the apparently simple translation observed here, and, since the mechanism refers to the instability of a single vortex, it provides no explanation for the apparent cooperative phenomenon observed in the experiment.

Pierrehumbert & Widnall (1982) have analysed the instability of a family of periodic vorticity distributions tailored to model the row of cores in the shear layer. The presence of many cores gives rise to two new cooperative instability modes. In the first one all the cores deform in phase along approximately the 45° line. The growth rate is zero both for uniform velocity distributions, lacking concentrated cores, and for very long wavelengths. For the model proposed by the authors as representative of real mixing layers there is a broad amplification band, for wavelengths between $0.25\,\lambda_2$ and $1.25\,\lambda_2$, for which the growth rate is only slightly lower than the one for the pairing interaction. This is very suggestive in view of the amplitude history presented in figure 14; as the layer leaves the nozzle lip with a velocity profile that is essentially uniform, the flow is two-dimensional; later, as the vorticity becomes concentrated in discrete cores, spanwise perturbations become unstable and both components grow at similar rates for a while. Since this moment corresponds roughly to the first pairing, it is difficult to decide which should be the initial spanwise wavelength. In our experiment we find between 1 and $2\,\lambda_{20}$, while Breidenthal gives approximately $1.2\,\lambda_{20}$; both values are inside the range predicted by the theory.

The second mode is a three-dimensional generalization of the classical pairing mechanism and is characterized by relatively long spanwise wavelengths. In fact, the fastest-growing mode is two-dimensional, and the authors suggest that the lack of amplification at high wavenumbers will result in the smoothing of pairing non-uniformities with wavelengths shorter than 3–$4\,\delta_\omega$. These wavelengths are quite longer than those in the corrugation, and both instabilities, even if present at the same time, probably interact weakly. In fact we have shown before that the scales given by Browand & Troutt for non-uniform pairings are very different from the ones of the corrugation, and that both phenomena are probably independent.

As the instability grows, linear analysis becomes inapplicable. Once longitudinal vorticity is introduced in the braid between two cores, it is quickly strained and

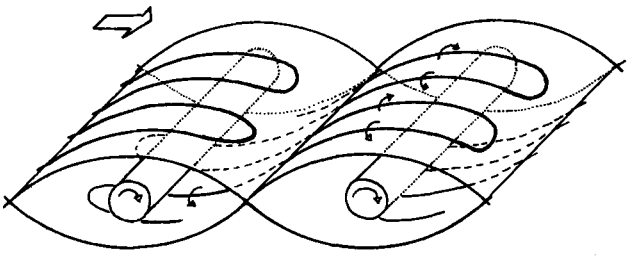

FIGURE 15. Tentative model for the nonlinear stage of the corrugation.

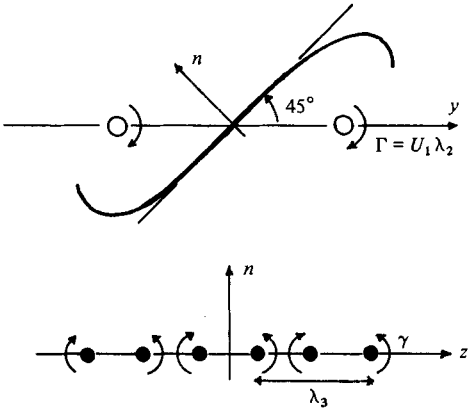

FIGURE 16. Geometry of the array of longitudinal vortices for the model used in text.

amplified (Corcos 1979), and the initial undulation is deformed into an array of longitudinal vortices of alternating signs. If these vortices are weak, they convect as essentially passive scalars, and eventually approach the streamlines bounding the cat's-eyes formed around the primary cores in the convection frame of reference. A similar, and somewhat more complete, conclusion was reached by Bernal (1981) using his visualization results. The resulting model is shown in figure 15.

Starting from this model it is possible to get an estimate of the circulation contained in the streamwise vortices. The easiest region to analyse is the neighbourhood of the stagnation point (in a frame moving with the cores) located between two cores. There, the braid, and the array of longitudinal vortices, lie almost in a plane inclined 45° to the stream direction. The vortex array will induce a periodic component in the x-direction which should correspond to the corrugation observed in the mean-velocity field. The geometry is shown in figure 16, and it is easy to show that the resulting r.m.s. intensity is

$$\sigma_3 = \frac{\delta_\omega \gamma}{4 U_1 \lambda_2}.$$

Using this formula, we get the results in figure 17. Disregarding the initial growth phase, in which the model of an array of compact vortex lines is not applicable, the circulation reaches a value and stays roughly constant. Moreover, this value is close to the circulation contained in the each of the two-dimensional cores formed in the initial primary instability and therefore is probably the value taken by the vortices at formation. It seems that the longitudinal vortices, once formed, do not amalgamate or decay appreciably. It is easy to see how an amalgamation of the primary structure

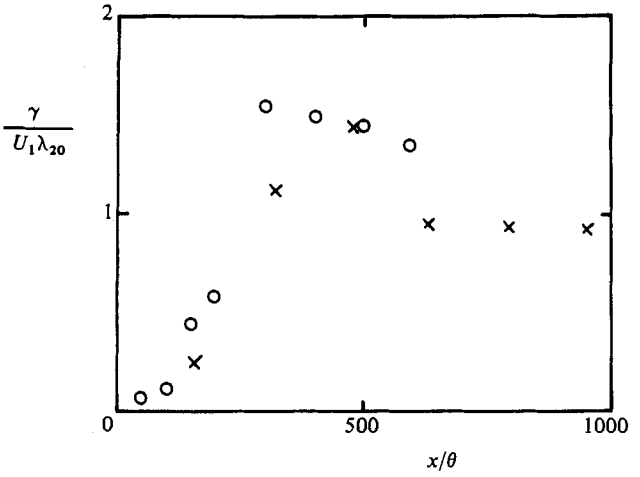

FIGURE 17. Circulation associated with the longitudinal vortices according to the model in text. For symbols see table 1.

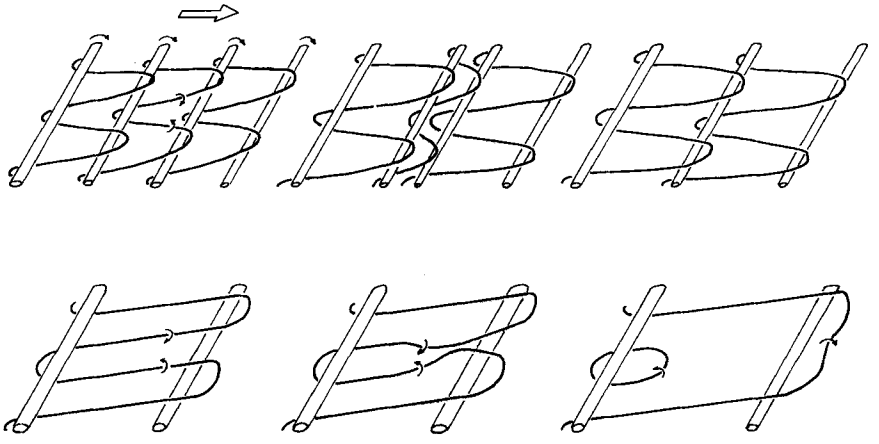

FIGURE 18. Proposed behaviour of the array of longitudinal vortices under amalgamation of the primary eddies (top), and disappearance of a vortex pair through pinching and cancellation (bottom). Time runs from left to right.

will leave the longitudinal vortices intact (see figure 18*a*). It is harder to understand how the spanwise wavelength can change without a corresponding change of circulation. A possible mechanism is sketched in figure 18(*b*). Since neighbouring vortices have opposite circulations, they will cancel each other as they amalgamate, leaving the other vortices in the array invariant. Such pinching interactions have been well documented in the counterrotating trailing vortices in airplanes (Crow 1970).

The last problem is whether the corrugation instability happens only once in the mixing layer or whether the spanwise cores continue to deform in later generations, producing stronger and stronger streamers. No evidence of more than one episode of instability was found in our experiment. However, any corrugation that is not locked to a fixed upstream influence will not be detected in our time-averaged measurements, and it is impossible, from the present evidence, to decide between the two possibilities. Although there are no theoretical results, there is some evidence in

the experiments of Konrad and Breidenthal that viscosity inhibits the corrugation instability; if this is the case, it is possible that turbulent dissipation in the cores also inhibits new instabilities in the downstream parts of the layer and that the organized three-dimensional structure proves to be a phenomenon localized to the transition regime.

A related question is what is the mechanism through which the flow chooses the spanwise wavelength in downstream locations? We have proposed above a way in which vortex lines can disappear, and, since it is easy to show that a linear array of alternating vortices is unstable, events of this or other types are bound to happen. There is, however, no theoretical argument that will fix the resulting wavelength at a value near δ_ω; the most-unstable wavelength predicted by theory is nearer $2\,\delta_\omega$, and relates to the formation of new undulations, instead of the reworking of old ones. That process would imply a periodic disintegration and reappearance of the streamers that is not very consistent with the picture in figure 9. Considerably more experimental and theoretical work are needed in this area.

6. Conclusions

We have shown that, under some conditions, the plane mixing layer develops a spanwise structure whose characteristics suggest that it is due to a secondary instability of the flow. The nature of the instability is a undulation of the vortex cores as a whole, and our results show that the deformation has a component transversal to the layer. Results presented by other investigators imply a longitudinal component, and the complete picture is probably a deformation in a plane inclined to the free-stream velocity, which later evolves into the longitudinal vortices observed by other investigators.

The evolution of the amplitude of the undulation is consistent with a model in which the instability depends on the previous establishment of concentrated vorticity cores. In natural layers, therefore, the deformation develops at the same time as the first pairing events; this makes it difficult to separate the effects of both phenomena on the establishment of a fully random three-dimensional flow, even if their interaction must be important in this respect. It is not clear, for example, whether the three known instabilities (roll-up, pairing and undulation) are enough to account for transition or whether a new mode must be invoked. Forcing experiments in which the modes are excited independently might contribute to clarify this point.

This work was supported in part by the London Office of the U.S. Army European Research Office and by the Spanish Comision Asesora de Investigacion.

REFERENCES

BENNEY, D. J. 1961 A non-linear theory for oscillations in a parallel flow. *J. Fluid Mech.* **10**, 209–236.

BERNAL, L. P. 1981 The coherent structure in turbulent mixing layers, II: Secondary streamwise vortex structure. PhD thesis, Caltech.

BERNAL, L. P., BREIDENTHAL, R. E., BROWN, G. L., KONRAD, J. H. & ROSHKO, A. 1979 On the development of three dimensional small scales in turbulent mixing layers. In *Proc. 2nd Symp. Turbulent Shear Flows, London*, pp. 8.1–8.6.

BREIDENTHAL, R. E. 1981 Structure in turbulent mixing layers and wakes using a chemical reaction. *J. Fluid Mech.* **116**, 1–24.

BROWAND, F. K. & TROUTT, T. R. 1980 A note on spanwise structure in the two-dimensional mixing layer. *J. Fluid Mech.* **97**, 771–781.

CORCOS, G. M. 1979 The mixing layer: Deterministic models of a turbulent flow. *Rep. FM-79-2 University of California, Berkeley.*

CROW, S. C. 1970 Stability theory for a pair of trailing vortices. *AIAA J.* **8**, 2172–2179.

HERNAN, M. A. & JIMENEZ, J. 1982 Computer analysis of a high-speed film of the plane turbulent mixing layer. *J. Fluid Mech.* **119**, 323–345.

HUSSAIN, A. K. M. F. & ZEDAN, M. F. 1978 Effects of the initial condition on the axisymmetric free shear layer: effects of the initial momentum thickness. *Phys. Fluids* **21**, 1100–1112.

JIMENEZ, J., MARTINEZ-VAL, R. & REBOLLO, M. 1979*a* The spectrum of the large scale structures in a mixing layer. In *Proc. 2nd Symp. Turbulent Shear Flows, London*, pp. 8.7–8.11.

JIMENEZ, J., MARTINEZ-VAL, R. & REBOLLO, M. 1979*b* The origin and evolution of three dimensional effects in the mixing layer. *USA-ERO Rep.* 79-G-079, *London.*

KONRAD, J. H. 1976 An experimental investigation of mixing in two-dimensional turbulent shear flows with applications to diffusion-limited chemical reactions. PhD thesis, Caltech.

KOOCHESFAHANI, M. M., CATHERASOO, C. J., DIMOTAKIS, P. E., GHARIB, M. & LANG, D. B. 1979 Two-point LDV measurements in a plane mixing layer. *AIAA J.* **17**, 1347–1351.

MICHALKE, A. 1965 On spatially growing disturbances in an inviscid shear layer. *J. Fluid Mech.* **23**, 521–544.

MOORE, D. W. & SAFFMAN, P. G. 1975 The instability of a straight vortex filament in a strain field. *Proc. R. Soc. Lond.* **A346**, 413–425.

PIERREHUMBERT, R. T. & WIDNALL, S. E. 1982 The two- and three-dimensional instabilities of a spatially periodic shear layer. *J. Fluid Mech.* **114**, 59–82.

ROSHKO, A. 1980 The plane mixing layer, flow visualization results and three dimensional effects. In *The Role of Coherent Structures in Modelling Turbulence and Mixing* (ed. J. Jimenez). Lecture Notes in Physics, vol. 136, pp. 208–217. Springer.

SAFFMAN, P. G. & BAKER, G. R. 1979 Vortex interactions. *Ann. Rev. Fluid Mech.* **11**, 95–122.

TSAI, C. Y. & WIDNALL, S. E. 1976 The stability of short waves on a straight vortex filament in a weak externally imposed strain field. *J. Fluid Mech.* **73**, 721–733.

WELCH, P. D. 1967 The use of FFT for estimation of power spectra. *IEEE Trans. Audio Electro.* **15**, 70–73.

WINANT, C. D. & BROWAND, F. K. 1974 Vortex pairing: the mechanism of turbulent mixing layer growth at moderate Reynolds number. *J. Fluid Mech.* **63**, 237–255.

WIDNALL, S. E., BLISS, D. B. & TSAI, C. Y. 1974 The instability of short waves in a vortex ring. *J. Fluid Mech.* **66**, 35–47.

WYGNANSKI, I., OSTER, D., FIEDLER, H. & DZIOMBA, B. 1979 On the perseverance of a quasi-two-dimensional eddy structure in a turbulent mixing layer. *J. Fluid Mech.* **93**, 325–335.